Ultra-Broadband Thermal Emitter for Daytime Radiative Cooling with Metal-Insulator-Metal Metamaterials

Huaiyuan Yin(殷怀远) and Chunzhen Fan(范春珍)*

School of Physics and Microelectronics, Zhengzhou University, Zhengzhou 450001, China

(Received 7 April 2023; accepted manuscript online 25 May 2023)

A novel thermal emitter with metal-insulator-metal design is proposed to realize efficient daytime radiative cooling. It can achieve ultrahigh absorption of 99.67% in the first atmospheric window and strong reflection of 94.86% in solar band. Analysis on the cooling performance with different real and imaginary parts of refractive index is carried out to provide a guide line in the material choice. As a case study, three inorganic materials are substituted to get enhanced absorption and it is verified that the refractive index matching is desirable to obtain high absorption. In addition, such high emissivity persists under different incident angles in both TE and TM modes. A net cooling power of 96.39 $\mathrm{W/m^2}$ is achieved in the daytime with the incorporation of convection coefficients. Finally, this thermal emitter achieves an average temperature drop of 5.1 ℃ based on the solution of conduction equation at 300 K. Therefore, our design with an excellent cooling ability can further bolster development in managements of radiative cooling or thermal radiation.

DOI: 10.1088/0256-307X/40/7/077801

With the increasing demand of energy consumption, the emission of greenhouse gas has posed a threat to our living environment. Traditional thermal management over the heat relies heavily on the electric power and inevitably requires a large amount of fossil fuels. An emerging field of thermal photonics provides an exciting opportunity to manipulate the radiative process to reduce the energy consumption.[1] Namely, a radiative cooling technology, which carries away thermal energy from the object spontaneously through the transparent windows without any consumption.[2] As early as 1977, Bartoli *et al.*[3] put forward the general physical principles involved in radiative cooling, enabling us to predict the cooling ability through the optical properties of the atmosphere and emitter surface.

Up to date, much progress has been achieved in research of radiative cooling. For example, Raman *et al.*[4] experimentally investigated a multilayer radiative cooler with the thermal photon method for the first time in 2014. It could reflect 97% of the incident sunlight and obtain a high emissivity in the transparent window. Kou *et al.*[5] proposed a fused silicon mirror with a polymer coating of polydimethylsiloxane (PDMS) on the top, achieving nearly ideal reflection in the solar band and perfect blackbody radiation in the mid-infrared band in 2017. Raphaeli *et al.*[6] explored the possibility of nano-photon structures for daytime radiative cooling with two layers of SiC and SiO_2 photonic crystal design. It experienced a decrease in temperature of 5 ℃ compared to the ambient temperature. Also, researchers[7,8] tailored surfaces with microstructures to control over thermal emission through the association of a grating and a multi-layer structure. Jia *et al.*[9] achieved enhanced radiative cooling performance of nanoparticle crystal via oxidation. In Ref. [10], Jia *et al.* obtained high emittance of 95.2% in the atmospheric window with phase change material. However, the narrow-band absorption in previous studies is contradictory to the wide band emission of radiative cooling. They usually took inorganic materials as absorbing mediums and the relevant metasurface was in the form of air slots.

Metal-insulator-metal (MIM) metamaterials can also be employed to achieve perfect absorption. If an absorption peak is adjusted into the atmospheric window, the principle of radiative cooling is satisfied. An MIM metamaterial is usually composed of three layers. The top metal metasurface, a middle dielectric layer, and a bottom continuous metallic substrate to eliminate wave transmittance and to enhance the absorption inside the absorber.[11–13] The thickness of an MIM absorber is usually much thinner than the subwavelength wave.[14] Kim *et al.*[15] proposed a dual-band metamaterial perfect absorption at 1.54 μm and 6.2 μm with MIM in the infrared stealth technology. Liu *et al.*[16] presented a novel multilayer MIM resonators periodically on a $PbTe/MgF_2$ bilayer substrate. Hossain *et al.*[17] proposed MIM-based broadband radiative coolers and extensively studied the selective IR emission.

In this work, an enhanced thermal emissivity in an atmospheric transparency window is achieved based on the MIM design. Influence of the dielectric layer on the enhanced absorption is considered with different real and imaginary parts. The optimized value is achieved when the real part of the intermediate medium is taken as 1.5 and the imaginary part is set as 0.6. An average high reflection of 94.86% and the average emissivity of 99.67% are achieved. The intermediate medium is replaced with TiO_2, SiO_2, and Si_3N_4 to evaluate the cooling capacity of the device. The average emissivity at different incident angle is explored and the cooling power is calculated at dif-

*Corresponding author. Email: chunzhen@zzu.edu.cn
© 2023 Chinese Physical Society and IOP Publishing Ltd

ferent coefficients. Finally, the geometry of surface metal is calibrated to obtain high emissivity.

Theory—Radiative Cooling Power. Based on the law of energy conservation, the radiative cooling power of thermal emitter is closely related to the external environment, the radiation in solar band, and the atmospherically thermal radiation. Net radiative cooling power $P_{\rm net}(T)$ is used to indicate the radiant capacity. It can be expressed as

$$P_{\rm net}(T) = P_{\rm rad}(T) - P_{\rm atm}(T_{\rm amb}) - P_{\rm sun}(T) - P_{\rm nonrad}(T). \quad (1)$$

The thermal cooling power $P_{\rm rad}(T)$ is written as

$$P_{\rm rad}(T) = A \int d\Omega \cdot \cos\theta \int_0^{\infty} d\lambda \cdot I_{\rm BB}(T,\lambda) \cdot e(\lambda,\theta), \quad (2)$$

where $I_{\rm BB}(T,\lambda)$ is the Planck black-body thermal radiation, and $e(\lambda,\theta)$ is the emission of the device.

The atmospheric radiation $P_{\rm atm}(T_{\rm amb})$ is expressed as

$$P_{\rm atm}(T_{\rm amb}) = \int d\Omega \cdot \cos\theta \int_0^{\infty} d\lambda \cdot I_{\rm BB}(T_{\rm amb},\lambda) \cdot e(\lambda,\theta) \cdot e_{\rm amb}(\lambda,\theta). \quad (3)$$

Here, T is the temperature of radiator; $T_{\rm amb}$ is the temperature of ambient environment and sets as 300 K; λ ranges from 8 to 13 μm in the atmospheric window; $e_{\rm amb}(\lambda,\theta)$ denotes the spectral directional emissivity of the atmosphere.

$$I_{\rm BB}(T,\lambda) = \frac{2\pi hc^2}{\lambda^5(e^{h_c/k_{\rm B}T\lambda}-1)}, \quad (4)$$

where h is the Planck constant, $h_{\rm c}$ is the the heat transfer coefficient of conduction and convection,[18] $k_{\rm B}$ is the Boltzmann constant, and $e(\lambda\theta)$ is the absorption spectrum of the radiator.[19]

$P_{\rm sun}$ equals the solar energy absorbed by the device in daytime.

$$P_{\rm sun}(T) = \int_0^{\infty} d\lambda \cdot I_{\rm AM}(\lambda) \cdot e(\lambda), \quad (5)$$

with $I_{\rm AM}(T,\lambda)$ being the solar radiance from 0.3 μm to 4 μm. The conduction and convective radiation $P_{\rm nonrad}(T)$ can be expressed as

$$P_{\rm nonrad}(T) = h_{\rm c}(T_{\rm amb} - T). \quad (6)$$

The correlation commonly used to estimate the convective heat transfer coefficient $h_{\rm c}$ is recommended by $h_{\rm c} = 1.44v + 4.955$, where $h_{\rm c}$ is in units of $\rm W{\cdot}m^{-2}{\cdot}K^{-1}$ and v is the wind speed in units of m/s. In the outdoor environment, since the wind speed is generally moderate, heat transfer coefficient varies from 6 to 10 $\rm W{\cdot}m^{-2}{\cdot}K^{-1}$.[20]

The average emissivity $\varepsilon(\lambda_1,\lambda_2)$ can be written as

$$\varepsilon(\lambda_1,\lambda_2) = \frac{\int_{\lambda_1}^{\lambda_2} e(\lambda,\theta) I_{\rm BB}(T,\lambda) d\lambda}{\int_{\lambda_1}^{\lambda_2} I_{\rm BB}(T,\lambda) d\lambda}. \quad (7)$$

Structure Design. The MIM metamaterial with cross-shaped surface is superimposed on the dielectric layer in Fig. 1. The unit cell periodically arrays along x and y axes. The periodicity is $P_x = P_y = 14$ μm. The width $w = 2$ μm and length $l = 6$ μm are also employed in Fig. 1(b). The intermediate layer is selected as an inorganic material with inherent loss in atmospheric window, which is transparent in solar band. It is commonly selected as SiO_2, TiO_2, or Si_3N_4. The bottom metal layer is taken as Ag and its dielectric function follows the Drude mode. The refraction index of the intermedium is expressed as $n + ik$. The thickness of each layer is set as $d_1 = 2$ μm, $d_2 = 2$ μm. Our numerical results of the radiative cooling device are carried out with commercial software COMSOL Multiphysics.[21] It subdivides a large system into smaller parts, and they are called finite elements. The simple equations are then assembled into a larger system to model the entire problem. With the continuity of the tangential electric field at each boundary, the parameters of the simulated space electromagnetism are all given in the space grid. To model our design, we first established a three-dimensional simulation domain, the reflectance $R_{\rm reflect}$ and transmittance $T_{\rm transmit}$ were then calculated by modeling the propagation of the incident plane wave in the normal z incident direction. Two integral planes were set above the surface of the incident light direction and below the bottom layer respectively. The perfectly matched layer was applied to the boundary along the propagation direction (z-axis) to eliminate the non-physical reflection at the boundary. Periodic conditions were taken to simplify the modeling. Free tetrahedrons and triangular meshes were selected to divide the domain and boundary of the calculated structure. Finally, the upper and lower boundaries of the structure were integrated to obtain the absorption α through the relationship $\alpha = 1 - R_{\rm reflect} - T_{\rm transmit}$. Thus, the calculated value is the integral value of energy through the surface. As it is an energy integral, the higher order diffraction is included by default. To prepare the proposed thermal emitter, we can resort to the physical vapor deposition method. Silver is taken as a substrate during deposition and the thickness of each layer can be precisely controlled to obtain the MIM metamaterial. A focused ion beam with resolution up to 4–5 nm is sufficient to prepare the patterned surface.[22] The metallic substrate in our design of the MIM metamaterial is mainly responsible for the reflection in the solar band. If the substrate is changed into a Au layer, the emissivity will not change. They are almost overlap in the transparency window.

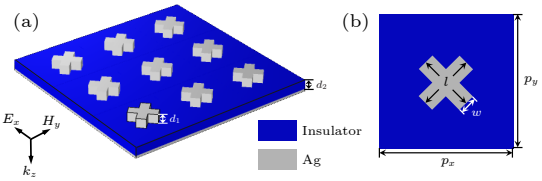

Fig. 1. Design of thermal emitter with the MIM metamaterial. (a) Cross shaped unit cells are arranged periodically in the x and y directions, $d_1 = 2$ μm, $d_2 = 2$ μm. (b) Top view of the unit cell, $P_x = P_y = 14$ μm, $l = 6$ μm, $w = 2$ μm.

Results and Discussions. The high reflection in solar band and strong absorption in atmospheric window is illustrated in Fig. 2. The real part of the intermediate medium is taken as 1.5 and the imaginary part is set as 0.6. The reflection of the MIM structure with an average reflection

of 94.86% is observed in Fig. 2(a), which reflects sunlight for cooling purposes. Meanwhile, an ultrahigh absorption in the atmospheric window is clearly observed in Fig. 2(b). The average emissivity is as high as 99.67%. For the lossy-free intermediate layer in the solar band, namely, the imaginary part is taken as zero, a slightly variation of the real part does not cause a significant change of the reflectivity. In addition, our numerical results indicate that increased thickness of the intermediate medium does not reduce the absorption, which also provides us one more modulation space in the material selection.[23,24] To obtain the temperature difference, a steady heat balance system is constructed. It consists of a radiative cooling thin film and it is placed high above the ground in an ideal atmospheric environment. The sun shines directly on the air-filled box. To calculate the cooling ability of the system, it is simplified as a three-layer system. The solution of the heat conduction equations is programmed using the Jacobi iteration method with the help of boundary conditions [see Fig. S1 in the Supplementary Material]. They are ended up with a temperature distribution at all locations. It can be concluded that the drop of temperature in the first atmospheric window is 5.1 ℃ from 300 K.[25] The broad band absorption in our radiative cooling design is mainly caused by the inherent absorption of the complex dielectric medium. The imaginary part of the refraction index dominates the broad band absorption. The surface pattern modulates the electric field distribution and the waveguide resonance to obtain a higher absorption.

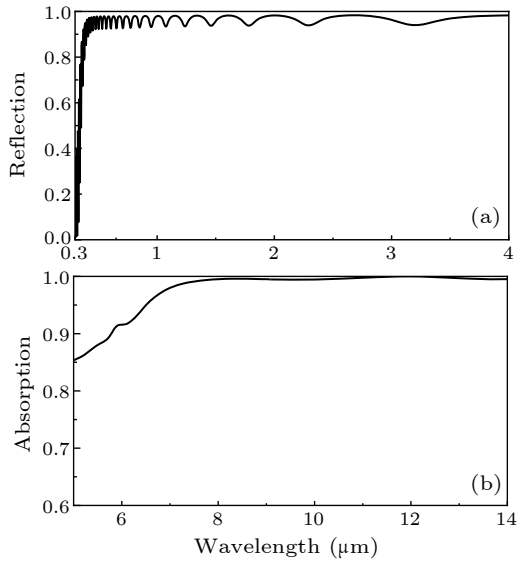

Fig. 2. Optical response in our proposed thermal metamaterial: (a) reflection in solar band, (b) absorption in the first atmospheric window.

The absorption with different intermediate mediums is elaborately studied in Fig. 3. The influence of real parts on the absorption is shown in Fig. 3(a) and the imaginary part of intermediate refractive index is fixed at 0.6. The maximum average emissivity is achieved when the real part equals 1.5. However, if the real part is taken as other values, it is necessary to adjust the thickness of the intermediate medium and the surface structure parameters to achieve high emissivity. Figures 3(b) and 3(c) illustrate the influence of imaginary part k on absorption spectrum with $n = 1.5$. The average emissivity first increases and then decreases when n is from 0.2 to 1.0. The average emissivity reaches a maximum when k is 0.6. A larger k leads to an increase of the phonon polarization resonance in the intermediate medium and thereby enhances the overall absorption. However, the reflection barely changes. The absorption of light through the medium is reduced at a larger k in Fig. 3(c). A higher loss is always accompanied with a high reflection. When the reflection plays a leading role, the overall absorption decreases. For the decreased part, the intermediate medium transforms towards metal with the further increased imaginary part. Therefore, the optimal refraction index of the intermedium is finally selected as $1.5 + 0.6i$ to get the highest emissivity.

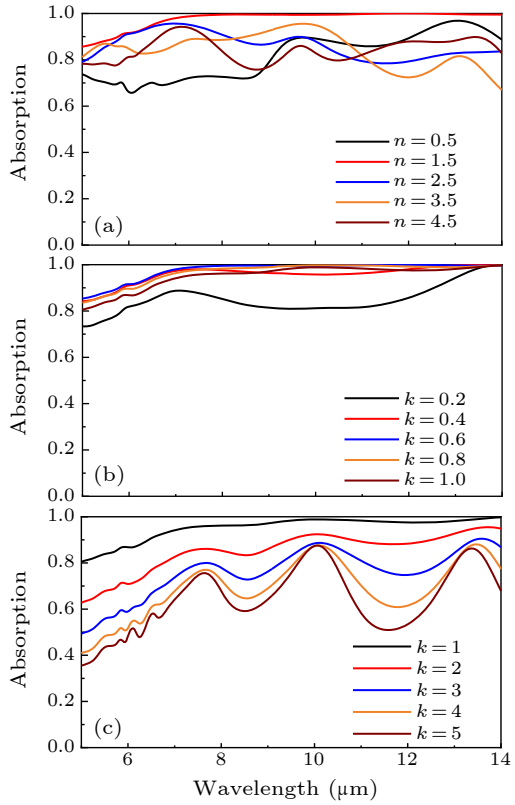

Fig. 3. Absorption versus wavelength with different real (n) and imaginary (k) parts of intermediate medium refractive index: (a) n is taken from 0.5 to 4.5 for $k = 0.6$, (b) k is taken from 0.2 to 1.0 for $n = 1.5$, (c) k is taken from 1 to 5 for $n = 1.5$.

To fully explore the physical origin of the high absorption in the atmospheric window, three resonant positions at 7.4 μm, 9.5 μm, 13.3 μm are marked in Fig. 4(a). When the intermediate medium is taken as Si_3N_4, there is a perfect absorption at 9.5 μm. The corresponding real and imaginary parts of the refractive index of Si_3N_4 at this point exactly locate near 1.5 and 0.6, which agrees well with the above analysis. We also selected two other wavelength positions at 7.4 μm and 13.3 μm for comparison. The electric field distribution in the top view indicates that there is a strong resonance around the surface metal-

lic unit cell and a relatively weak dipole resonance during one period in Figs. 4(b)–4(f). Figures 4(c)–4(g) illustrate that the electric field decreases from top to bottom. Therefore, the strongest electric field is located around the surface unit cell and rapidly decays in the middle Si_3N_4 layer. The bottom metal layer blocks the downward propagating incident wave.

The refraction index is wavelength dependent and three mediums of Si_3N_4, SiO_2, and TiO_2 with high intrinsic absorption are taken as the intermedium layer. Their average emissivity in radiative cooling is listed for comparison in Table 1. The thickness of the intermedium is considered from 2 to 7 μm. The average emissivity is larger in the design of the MIM metamaterial and it increases monotonously with a thicker intermedium. To show the superiority of the MIM structure, the corresponding emissivity of the Si_3N_4 unit cell (the second row) and double-layer design (the third row) are also investigated. These calculated results show that the patterned metallic unit cell can effectively increase the average emissivity. When the thickness of the medium is small, the average emissivity of Si_3N_4 is the highest. When the thickness is larger than 6 μm, the average emissivity of TiO_2 increases rapidly and achieves the highest absorption. In order to reduce the overall thickness of the device, Si_3N_4 is chosen as the intermedium to calculate cooling power and cooling rate.

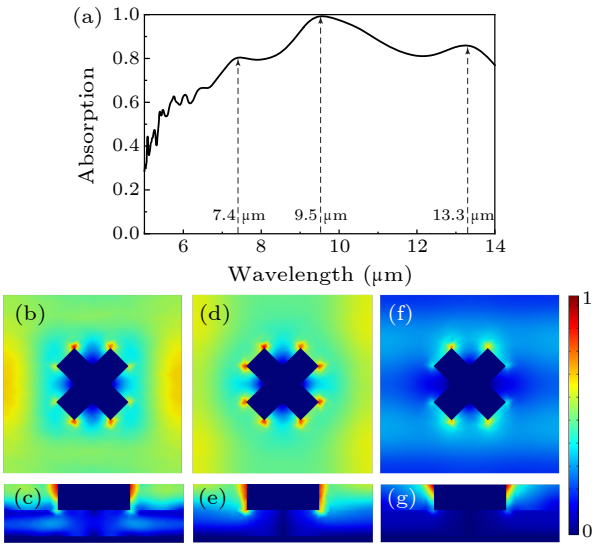

Fig. 4. (a) Absorption of optimal MIM design when the intermediate layer is set as Si_3N_4. (b)–(f) Top views of electric field distribution at 7.4 μm, 9.5 μm, and 13.3 μm. (c)–(g) Side views of electric distribution at 7.4 μm, 9.5 μm, and 13.3 μm.

Table 1. Average emissivity in the design with different intermediums and thicknesses.

Thickness (μm)	2	3	4	5	6	7	8	9	10
M–Si_3N_4–M	0.886	0.912	0.913	0.916	0.917	0.919	0.92	0.921	0.923
Si_3N_4–Si_3N_4–M	0.836	0.861	0.862	0.866	0.866	0.868	0.869	0.870	0.874
Si_3N_4–M	0.717	0.748	0.753	0.758	0.76	0.762	0.764	0.764	0.769
M–TiO_2–M	0.767	0.845	0.876	0.909	0.925	0.933	0.946	0.950	0.961
M–SiO_2–M	0.703	0.752	0.816	0.853	0.838	0.856	0.880	0.879	0.880

The average emissivity at different incident angles in both TE and TM modes are explored in Fig. 5. The average emissivity of the MIM structure is different from that of the conventional radiative cooler at a larger incident angle. For the MIM structure, electromagnetic wave will generate high-order spatial resonance in the middle cavity when the incident angle is varied, resulting in a new absorption. Thus, the average emissivity of TM mode is lower than that of TE mode. In addition, the overall emissivity is higher when the thickness of the intermediate medium is taken as 3 μm.

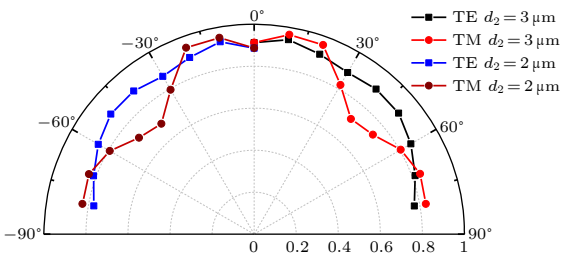

Fig. 5. The average emissivity with different incident angles in both TE and TM polarizations when the thickness of the intermedium Si_3N_4 is taken as 2 μm and 3 μm, respectively.

Figure 6 shows the cooling power at different temperatures when the thickness of the intermediate layer is 2 μm (dotted line) and 3 μm (solid line). P_{rad} is the total radiation power without considering the influence of atmospheric, P_{night} is the net power at night, and P_{day} is the cooling power incorporating the absorbed sunlight in Fig. 6(a). Cooling power increases at a higher temperature. When the temperature is 300 K, the net cooling power is 96.39 W/m^2. Figure 6(b) shows the cooling power at different convection coefficients h_c (from 0 $W{\cdot}m^{-2}{\cdot}K^{-1}$ to 9 $W{\cdot}m^{-2}{\cdot}K^{-1}$). The value of h_c is proportional to the heat exchange between the object and surroundings.[26,27] It can be clearly observed that the cooling power is enhanced at a larger h_c.

The average emissivity with different geometric parameters of top unit cell is depicted in Fig. 7. The real part of the intermediate medium refractive index is 1.5 and the imaginary part is 0.6. The surface metallic unit cell with the optimal geometric parameters ($d_1 = 2$ μm, $w = 2$ μm, $l = 6$ μm) makes the final average emissivity highest. Under this circumstance, the emitter can achieve the highest cooling effect. The corresponding average emissivity is 99.67%, achieving nearly perfect absorption of wide band within the first atmospheric window. Small variation of the geometry parameters will lead to a reduced emissivity.

Therefore, the physical parameters of top unit cell need to be precisely controlled in the manufacturing process.

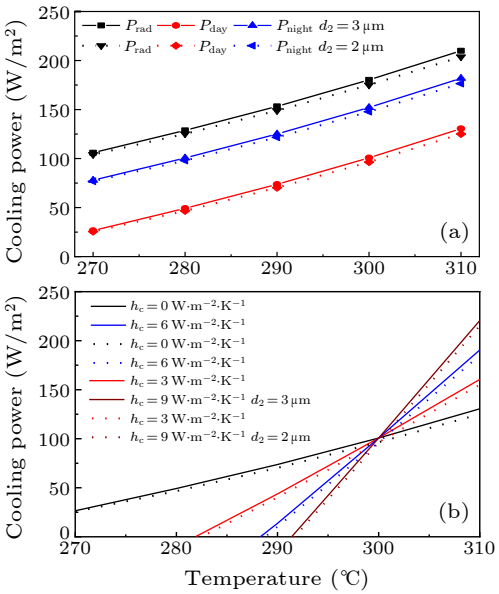

Fig. 6. Cooling power at different thicknesses of the intermedium: (a) radiative cooling power of our designed thermal emitter ($P_{\rm rad}$), the cooling power in the daytime ($P_{\rm day}$) and night time ($P_{\rm night}$) versus temperature, (b) cooling power with different convection coefficients $h_{\rm c}$.

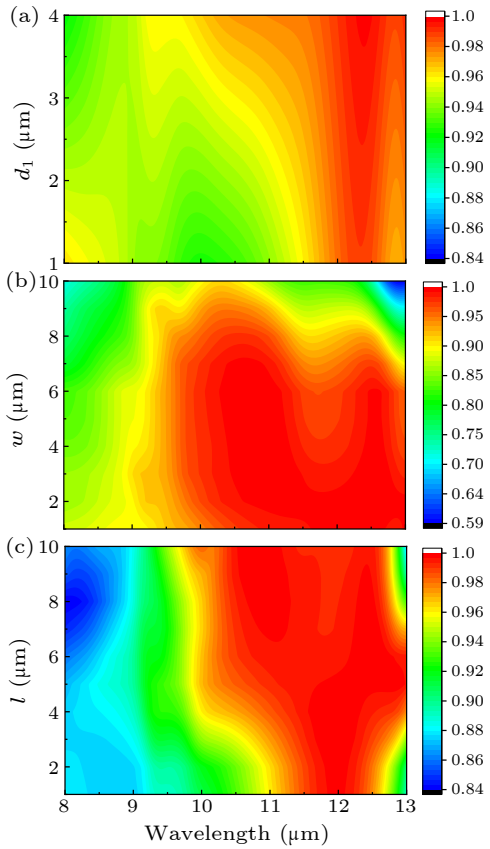

Fig. 7. Average emissivity with different geometric parameters of top unit cell: (a) d_1, (b) w, (c) l.

Finally, we compare the cooling ability of our thermal emitter with published literature in Table 2.

Table 2. The comparison of cooling power and emissivity with other work.

References	Emissivity	Cooling power
[28]	78%	35 W/m^2
[29]	91%	106 W/m^2
[30]	>90%	52 W/m^2
[31]	>80%	100 W/m^2
[16]	$\sim$90%	114 W/m^2 (night time)
Our work	99.67%	96.39 W/m^2 147.79 W/m^2 (night time)

For our radiative cooling device, the average high emissivity of 99.67% is achieved in the first atmospheric window, which is higher compared with other results.[28–31] The value of cooling power depends on the reflection of the solar band no matter whether we take the second atmospheric window into consideration. Our cooling power is 96.39 W/m^2 in the daytime and it is 147.79 W/m^2 in the night time. Although the cooling power is lower in the daytime, the nighttime cooling power is the largest. In addition, the conventional multilayer devices are commonly used to realize a high emissivity for efficient cooling, the introduction of intermediate inorganic absorbing medium in the MIM structure can greatly lower the cost and make it easy to fabricate in the lab.

In summary, an MIM thermal emitter is designed to achieve enhanced emissivity for radiative cooling. The influence of the real and imaginary part of the intermedium is elaborately analyzed. It is found that our design can achieve high absorption in the atmospheric window when Si_3N_4 is selected, which is consistent with the analysis of $1.5 + 0.6i$. The impacts of intermedium types, structural parameters and incident angle on the general average emission are also investigated. A high cooling power of 96.39 W/m^2 is achieved in the daytime with the incorporation of convection coefficients, which is desirable in the radiative cooling application and other related fields with a simple MIM design.[16]

Acknowledgments. This work was supported by the Natural Science Foundation of Henan Educational Committee (Grant No. 21A140026), the Natural Science Foundation of Henan Province (Grant Nos. 212300410411 and 232102231023), the National Natural Science Foundation of China (Grant No. 12174351), and the Fund from Zhengzhou University (Grant No. JC22149003).

References

[1] Fan S H and Li W 2022 *Nat. Photon.* **16** 182
[2] Ono M, Chen K F, Li W, and Fan S H 2018 *Opt. Express* **26** A777
[3] Bartoli B, Catalanotti S, Coluzzi B, Cuomo V, Silvestrini V, and Troise G 1977 *Appl. Energy* **3** 267
[4] Raman A P, Anoma M A, Zhu L X, Rephaeli E, and Fan S H 2014 *Nature* **515** 540
[5] Kou J L, Jurado Z O, Chen Z, Fan S H, and Minnich A J 2017 *ACS Photon.* **4** 626
[6] Rephaeli E, Raman A P, and Fan S 2013 *Nano Lett.* **13** 1457
[7] Hervé A, Drévillon J, Ezzahri Y, and Joulain K 2018 *J. Quant. Spectrosc. Radiat. Transfer* **221** 155

[8] Liu T J and Takahara J 2017 *Opt. Express* **25** A612
[9] Jia Z X, Shuai Y, Li M, Guo Y M, and Tan H P 2018 *J. Quant. Spectrosc. Radiat. Transfer* **207** 23
[10] Jia Y L, Wang X X, Yin H Y, Yao H W, Wang J Q, and Fan C Z 2021 *Appl. Opt.* **60** 5699
[11] Wang J H and Fan C Z 2022 *Opt. Mater.* **134** 113131
[12] Cui Y X, Fung K H, Xu J, Ma H, Jin Y, He S, and Fang N X 2012 *Nano Lett.* **12** 1443
[13] Contractor R, D'Aguanno G, and Menyuk C 2018 *Opt. Express* **26** 24031
[14] Jia Y L, Yin H Y, Yao H W, Wang J Q, and Fan C Z 2021 *Results Phys.* **25** 104301
[15] Kim J Y, Han K, and Jae W H 2017 *Sci. Rep.* **7** 6740
[16] Liu Y N, Weng X L, Zhang P, Li W X, Gong Y, Zhang L, Han T C, Zhou P H, and Deng L J 2021 *Chin. Phys. Lett.* **38** 034201
[17] Hossain M M, Jia B, and Gu M 2015 *Adv. Opt. Mater* **3** 1047
[18] Xu L J and Huang J P 2023 *Transformation Thermotics and Extended Theories inside and outside Metamaterials* (Singapore: Springer) p 9
[19] Huang J P 2020 *Theoretical Thermotics Transformation Thermotics and Extended Theories for Thermal Metamaterials* (Singapore: Springer) pp 231–242
[20] Paman R A, Li W, and Fan S H 2019 *Joule* **3** 2679
[21] Dickinson E J F, Ekström H, and Fontes E 2014 *Electrochem. Commun.* **40** 70
[22] Watt F, Bettiol A, Kan J A, Teo E, and Breese M 2005 *Int. J. Nanosci.* **4** 269
[23] Kong A, Cai B Y, Shi P, and Yuan X C 2019 *Opt. Express* **27** 30102
[24] Wu D, Li C, Xu Z H, Liu Y M, Yu Z Y, Yu L, Chen L, Li R F, Ma R, and Des Y H M 2018 *Mater. Design* **139** 104
[25] Yin H Y and Fan C Z 2023 *Results Phys.* **45** 106216
[26] Yin H Y, Yao H W, Jia Y L, Wang J Q, and Fan C Z 2021 *J. Phys. D* **54** 345501
[27] Yao H W, Wang X X, Yin H Y, Jia Y L, Gao Y, Wang J Q, and Fan C Z 2021 *Chin. Phys. B* **30** 064214
[28] Kecebas M A, Menguc M P, Kosar A, and Sendur K 2017 *J. Quant. Spectrosc. Radiat. Transfer* **198** 179
[29] Liu Y T, Son S, Chae D, Jung P H, and Lee H 2020 *Sol. Energy Mater. Sol. Cells* **213** 110561
[30] Huang Z and Ruan X 2017 *Int. J. Heat Mass Transfer* **104** 890
[31] Nilsson T M J, Niklasson G A, and Granqvist C G 1992 *Sol. Energy Mater. Sol. Cells* **28** 175